https://doi.org/10.1093/plcell/koac210 THE PLANT CELL 2022: 00: 1–14

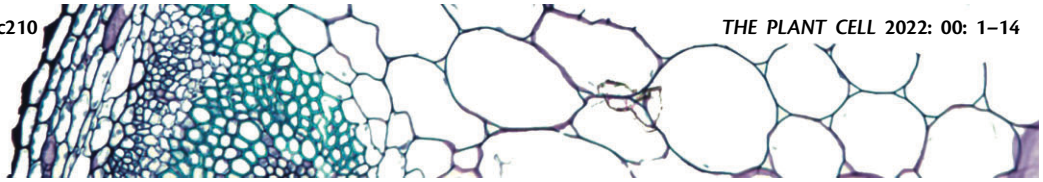

Breakthrough Report

A nuclear import pathway exploited by pathogenic noncoding RNAs

Junfei Ma [1], Shachinthaka D. Dissanayaka Mudiyanselage [1], Woong June Park [2], Mo Wang [3,4], Ryuta Takeda [5], Bin Liu [1] and Ying Wang [1,*]

1 Department of Biological Sciences, Mississippi State University, Starkville, Mississippi 39762, USA
2 Department of Molecular Biology, Dankook University, Chungnam 31116, Korea
3 Fujian University Key Laboratory for Plant-Microbe Interaction, Fujian Agriculture and Forestry University, Fuzhou 350002, China
4 College of Agriculture, Key Laboratory of Ministry of Education for Genetics, Breeding and Multiple Utilization of Crops, Fujian Agriculture and Forestry University, Fuzhou 350002, China
5 Leave a Nest Co., Ltd., Tokyo 162-0822, Japan

*Author for correspondence: wang@biology.msstate.edu

R.T. and Y.W. conceived the study. Y.W. designed the experiments. J.M., S.D.M., and Y.W. performed the experiments. J.M. and Y.W. analyzed the data. Y.W. wrote the manuscript. M.J., W.J.P., M.W., B.L., and Y.W. discussed the results and revised the manuscript.
The author responsible for distribution of materials integral to the findings presented in this article in accordance with the policy described in the Instructions for Authors (https://academic.oup.com/plcell) is: Ying Wang (wang@biology.msstate.edu).

Abstract

The prevailing view of intracellular RNA trafficking in eukaryotic cells is that RNAs transcribed in the nucleus either stay in the nucleus or cross the nuclear envelope, entering the cytoplasm for function. However, emerging evidence illustrates that numerous functional RNAs move in the reverse direction, from the cytoplasm to the nucleus. The mechanism underlying RNA nuclear import has not been well elucidated. Viroids are single-stranded circular noncoding RNAs that infect plants. Using *Nicotiana benthamiana*, tomato (*Solanum lycopersicum*), and nuclear-replicating viroids as a model, we showed that cellular IMPORTIN ALPHA-4 (IMPa-4) is likely involved in viroid RNA nuclear import, empirically supporting the involvement of Importin-based cellular pathway in RNA nuclear import. We also confirmed the involvement of a cellular protein (viroid RNA-binding protein 1 [VIRP1]) that binds both IMPa-4 and viroids. Moreover, a conserved C-loop in nuclear-replicating viroids serves as a key signal for nuclear import. Disrupting C-loop impairs VIRP1 binding, viroid nuclear accumulation, and infectivity. Further, C-loop exists in a subviral satellite noncoding RNA that relies on VIRP1 for nuclear import. These results advance our understanding of subviral RNA infection and the regulation of RNA nuclear import.

Introduction

Most cellular RNAs are produced through transcription in the nucleus of eukaryotic cells and the prevailing view is that those RNAs stay in the nucleus or move to the cytoplasm for function. However, emerging evidence shows that cellular RNAs (i.e. small RNAs, tRNAs, and rRNAs), as well as viral RNAs, can traffic in the reverse direction from the cytoplasm to the nucleus. For instance, plant 24-nucleotide (nt) heterochromatic small interfering RNAs are exported to the cytoplasm for ARGONAUTE 4 loading before being redirected into the nucleus of the same cell or even neighboring cells for RNA-directed DNA methylation (Ye et al., 2012; Long et al., 2021). In *Xenopus* oocytes, 5S rRNA relies on ribosomal protein L5 for nuclear import (Rudt and Pieler, 1996). In another example, satellite RNA of Q-strain cucumber mosaic virus (Q-satRNA) relies on a bromodomain-containing

Received June 07, 2022. Accepted July 18, 2022. Advance access publication July 25, 2022

IN A NUTSHELL

Background: During the course of evolution, eukaryotic cells gained a nuclear envelope to protect their genomes. However, to coordinate diverse biological processes, cellular contents need to communicate between the nucleus and the cytoplasm. The nuclear/cytoplasmic shuttling of proteins has been well studied, but only the nuclear export of RNAs has been analyzed in detail. Nevertheless, increasing evidence has shown that multiple functional RNAs traffic from the cytoplasm to the nucleus, by a yet-to-be-elucidated mechanism.

Questions: How can RNA be recognized for nuclear import? Which cellular proteins serve as vehicles for RNA nuclear import?

Findings: We used a pathogenic noncoding RNA (potato spindle tuber viroid [PSTVd]) as a model to study RNA nuclear import and found a particular RNA structure (C-loop) that is critical for PSTVd nuclear accumulation. PSTVd C-loop is recognized and bound by the cellular viroid RNA-binding protein 1 (VIRP1). Since nuclear import of proteins often relies on Importin, we performed a screen and identified IMPORTIN ALPHA-4 (IMPa-4) in a complex with PSTVd. Reducing the amount of IMPa-4 in cells inhibited PSTVd nuclear accumulation and infectivity. Interestingly, VIRP1 also relies on IMPa-4 for nuclear accumulation. Therefore, we propose a model that IMPa-4 transports the VIRP1–PSTVd complex into the nucleus. Notably, nearly all nuclear-replicating viroids and a viral satellite RNA contain a C-loop, suggesting that the C-loop is a conserved signal for RNA nuclear import.

Next steps: We are interested in identifying the C-loop structure in cellular RNAs. Once we find cellular RNAs with a C-loop, we will test whether those cellular RNAs are transported into the nucleus and explore the biological significance of their nuclear import.

cellular protein (viroid RNA-binding protein 1 [VIRP1]) for entering the nucleus (Chaturvedi et al., 2014). In contrast to the well-studied RNA nuclear export process, the RNA nuclear import machinery and mechanism remain obscure, particularly regarding the molecular basis underlying the specific selection of RNAs for nuclear import.

To cross the double-membrane nuclear envelope, biomolecules need to traffic through the highly organized nuclear pore complexes (NPCs) in eukaryotic cells (Merkle, 2011). NPCs are conserved in eukaryotic organisms with some variations (Xu and Meier, 2008; Meier and Brkljacic, 2009). Except for some free-diffusing small molecules below 40–60 kDa, most biomolecules rely on nuclear transport receptors (NTRs) to traffic through NPCs (Frey et al., 2006; Stewart et al., 2007; Frey and Gorlich, 2009; Merkle, 2011). Importin alpha subunits (IMPas) constitute a group of adapter proteins linking specific cargos to NTRs for crossing NPCs (Merkle, 2011). In *Arabidopsis thaliana*, nine IMPas play distinct yet partially redundant roles (Merkle, 2011; Chen et al., 2020). Whether any IMPa is involved in RNA nuclear import remains to be determined.

Viroids are single-stranded circular noncoding RNAs that infect plants (Wang, 2021). Due to their noncoding nature, viroids must utilize RNA structures to exploit cellular factors and complete their infection cycles. RNA secondary structures are primarily composed of helices and loops. RNA loops often form 3D structural motifs that contain highly arrayed non-Watson-Crick–Watson-Crick (non-WC–WC) base pairings and other base-specific interactions, including base stacking and base backbone interactions (Wang et al., 2018; Ma and Wang, 2022). Each RNA base can use its three edges (i.e. WC, Hoogsteen, and sugar edges) to form non-WC–WC base pairing geometries within a structural motif (Wang et al., 2018; Ma and Wang, 2022). Those non-WC–WC base pairings have been well documented in a large amount of atomic resolution crystallography and NMR spectroscopy data (deposited in Protein Data Bank; https://www.rcsb.org).

Several homology-based programs have been developed facilitating search for possible base-pairing geometry of a motif of interest (Sarver et al., 2008; Zirbel et al., 2015). The RNA Basepair Catalog summarizes all possible non-WC–WC base pairings and their similarities from the deposited structural data (Stombaugh et al., 2009), providing a valuable resource for analyzing non-WC–WC base pairings and for predicting functional substitutions (Wang et al., 2018). Such an approach, in combination with functional mutagenesis-based genetic analyses, has been successfully applied to analyze the structure–function relationships of multiple viroid motifs (Zhong et al., 2006, 2007; Takeda et al., 2011, 2018; Wu et al., 2019).

Viroid RNA secondary structures have been well annotated via various chemical mapping assays (Gast et al., 1996; Xu et al., 2012; Giguere et al., 2014; Giguere and Perreault, 2017), providing a solid foundation to annotate base interaction geometries within loop motifs. A genome-wide analysis of potato spindle tuber viroid (PSTVd) RNA motifs has identified 11 out of 27 loop motifs responsible for systemic infection (Zhong et al., 2008). Some of those loop motifs regulate RNA trafficking across certain cellular boundaries, and their 3D structures have been successfully annotated using a combination of program prediction and functional mutagenesis-based genetic approach (Zhong et al., 2007; Takeda et al., 2011, 2018; Wu et al., 2019). However, whether

any RNA motif regulates viroid subcellular localization and organelle targeting remains unknown. Viroids of the family *Pospiviroidae* all replicate in the nucleus, and their nuclear import process is highly regulated (Woo et al., 1999; Seo et al., 2020). Hence, their noncoding RNA genomes probably contain the necessary information in certain forms (e.g. an RNA 3D motif) to guide nuclear import. The cellular factor(s) for viroid nuclear import remains elusive as well. The VIRP1 has been suggested to accelerate the import of citrus exocortis viroid (CEVd), a relative of PSTVd within the same genus, to nuclei of onion (*Allium cepa*) cell strips (Seo et al., 2021). Nevertheless, whether and how VIRP1 regulates viroid nuclear import await to be clarified.

To gain a better understanding of RNA nuclear import, we identified *A. thaliana* IMPORTIN ALPHA-4 (IMPa-4) as a cellular factor that can enrich PSTVd through RNA immunoprecipitation. Sl *IMPa-4*, the *IMPa-4* ortholog in tomato (*Solanum lycopersicum*), a host plant of PSTVd, is critical for infection. We also demonstrated the interaction between IMPa-4 and VIRP1, which likely regulates VIRP1 nuclear import. Moreover, we observed that VIRP1 recognizes a specific RNA 3D motif, C-loop. C-loop was found in PSTVd and hop stunt viroid (HSVd), which belong to distinct genera. Mutational analyses showed that viroid C-loop is critical for VIRP1 binding, viroid nuclear accumulation and infectivity. Notably, C-loop can be found in nearly all nuclear-replicating viroids and also in the satellite RNA of Q-strain cucumber mosaic virus (Q-satRNA) that relies on VIRP1 for nuclear import. Therefore, this work provides insights into the biology of subviral RNAs. In addition, our data unravel a cellular pathway for RNA nuclear import and the molecular basis of a nuclear import signal in RNAs, which have significant implications in understanding the intracellular trafficking of viral RNAs, and potentially cellular RNAs as well.

Results

IMPa-4 is responsible for PSTVd nuclear import

Arabidopsis thaliana contains the necessary machinery to support PSTVd nuclear import and replication but repels PSTVd systemic infection (Daros and Flores, 2004; Jiang et al., 2019). To test whether any IMPa protein(s) is responsible for viroid nuclear import, we employed the RNA immunoprecipitation assay to test the possibility for PSTVd associating with any of the nine Arabidopsis IMPa proteins in a complex. We transiently expressed IMPa proteins via agroinfiltration in PSTVd-infected *Nicotiana benthamiana* plants for the RNA immunoprecipitation assay. As shown in Figure 1A, only IMPa-4 could specifically and consistently enrich PSTVd, as revealed by the presence of PSTVd in the immunoprecipitated fractions via reverse transcription (RT)-PCR. We chose *Histone H2A* mRNA (*Niben101Scf01866g00004.1*) as a negative control for RT-PCR because mRNAs cannot traffic back to the nucleus. Moreover, the *H2A* ortholog in tomato did not change expression level in PSTVd- or virus-induced gene silencing vector (tobacco rattle virus [TRV])-infected plants in our previous studies (Zheng et al., 2017b, 2017a). As shown in Figure 1A, IMPa-4 did not bind to the *Histone H2A* mRNA, supporting the specificity of IMPa-4 in forming a complex with PSTVd.

We then analyzed *IMPa* homologs in tomato, a host plant of PSTVd. Homology-based analysis revealed five genes: Sl *IMPa-1*, Sl *IMPa-2*, Sl *IMPa-3*, Sl *IMPa-4*, and Sl *IMPa-9* (Supplemental Table S1). Their expression was not significantly changed upon infection of PSTVd or TRV vector (Supplemental Table S1) (Zheng et al., 2017b, 2017a). Therefore, we employed virus-induced gene silencing to specifically downregulate the expression of Sl *IMPa-4* and tested PSTVd infection therein to corroborate the role of IMPa-4 in PSTVd infection. TRV^{GFP} served as a control that did not affect PSTVd infectivity (Figure 1B). We cloned an *IMPa-4*-specific fragment based on the BLAST result and constructed $TRV^{IMPa\text{-}4}$. As expected, the $TRV^{IMPa\text{-}4}$ construct transiently suppressed *IMPa-4* expression, which led to significant reduction of PSTVd accumulation in systemic leaves (Figure 1B).

We then used whole-mount in situ hybridization to analyze the quantity of PSTVd-infected nuclei in tomato systemic leaves. Whole-mount in situ hybridization is a well-established approach for visualizing viroid-infected nuclei thanks to the high concentration of viroid RNAs in the nucleus (Zhu et al., 2002; Qi et al., 2004; Zhong et al., 2007; Takeda et al., 2011). We found that systemic leaves from PSTVd and $TRV^{IMPa\text{-}4}$ co-inoculated plants showed very few PSTVd-infected nuclei, which contrasts with the presence of numerous PSTVd-infected nuclei in the systemic leaves co-inoculated with PSTVd and TRV^{GFP} (Figure 1C). These data suggest that IMPa-4 likely facilitates viroid nuclear imports in plants.

VIRP1 interacts with IMPa-4 for nuclear import

VIRP1 was discovered through screening a cDNA library from PSTVd-infected tomato for RNA ligand binding (Martinez de Alba et al., 2003) and was shown to affect viroid trafficking (Maniataki et al., 2003) and replication (Kalantidis et al., 2007). Downregulation of *VIRP1* expression is known to attenuate viroid replication in cells (Kalantidis et al., 2007). Recent progress showed that *VIRP1* is responsible for the nuclear import of Q-satRNA (Chaturvedi et al., 2014). However, whether *VIRP1* is responsible for viroid nuclear import remains elusive. If this is true, VIRP1 will likely function in the same pathway as IMPa-4.

To test this possibility, we first analyzed the role of IMPa-4 in regulating VIRP1 nuclear import. We infected *N. benthamiana* plants with TRV^{vector} or $TRV^{IMPa\text{-}4}$ via agroinfiltration. After verifying infection 2-week postinoculation (Figure 1D), we then transiently expressed LIKE HETEROCHROMATIN PROTEIN 1 (LHP1)-GFP or VIRP1-GFP in those plants via agroinfiltration. LHP1 relies on the redundant function of IMPa-1, IMPa-2, and IMPa-3 for nuclear import (Chen et al., 2020). As shown in Figure 1E, LHP1-GFP displayed similar fluorescence signals between plants infected with TRV^{vector} and $TRV^{IMPa\text{-}4}$. In contrast, VIRP1-GFP had relatively higher fluorescence signals in

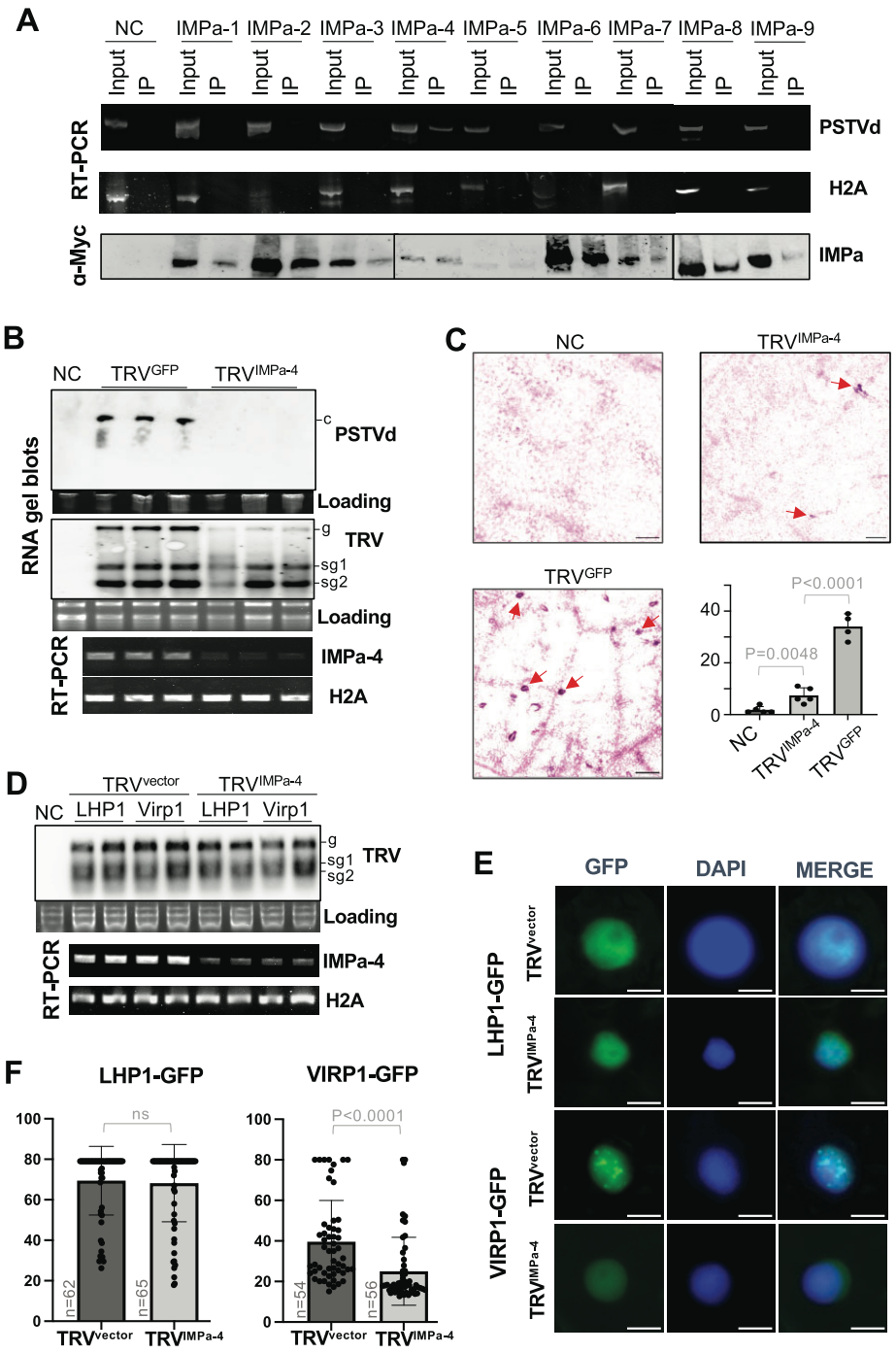

Figure 1 IMPa-4 and VIRP1 in the same pathway for PSTVd infection. A, RNA immunoprecipitation. *IMPa* genes were fused with a TAP-tag, which contains 9X cMyc, 2X IgG binding domain, and 1X His6. *IMPa* genes were transiently expressed in PSTVd-infected *N. benthamiana* plants via agro-infiltration and then harvested for immunoprecipitation using magnetic IgG beads. RNAs in the immunoprecipitation were subject to RT-PCR followed by electrophoresis using native PAGE gels. *Histone H2A* serves as a negative control. NC, infiltration with agrobacterium harboring no construct. IP, immunoprecipitated fraction. B, Virus-induced gene silencing of *IMPa-4* inhibiting PSTVd systemic infection in tomato. RNA gel blots showing PSTVd and TRV accumulation in infiltrated leaves. RT-PCR shows the specific downregulation of *IMPa-4* expression by the TRV^{IMPa-4} construct. "c" depicts circular genomic PSTVd. G, sg1, and sg2 indicate the genomic RNA1, subgenomic1 from RNA1, and subgenomic2 from RNA1, respectively. NC, tomato without PSTVd or TRV inoculation. C, Virus-induced gene silencing inhibiting PSTVd nuclear accumulation in systemic leaves. Whole-mount in situ hybridization showed that PSTVd-infected nuclei were significantly more in the systemic leaves of TRV^{GFP} inoculated tomato but not TRV^{IMPa-4} inoculated plants. NC, tomato without PSTVd or TRV inoculation. Scale bar, 40 μm. Quantitative analysis of PSTVd-infected nuclei in similar visual areas from four to five plants of each treatment. Two-tailed *t* test was performed using the built-in function in Prism. Virus-induced gene silencing inhibiting IMPa-4 expression in systemic leaves of *N. benthamiana* plants (D) and reducing VIRP1-GFP but not LHP1-GFP accumulation in the nucleus (E). NC, *N. benthamiana* plants without TRV inoculation. DAPI staining marks the nucleus. Scale bar, 8 μm. F, Statistical analysis of nuclear GFP signal showing that VIRP1-GFP but not LHP1-GFP reduced accumulation in the nucleus of plants with suppressed expression of *IMPa-4*. ns, not significant.

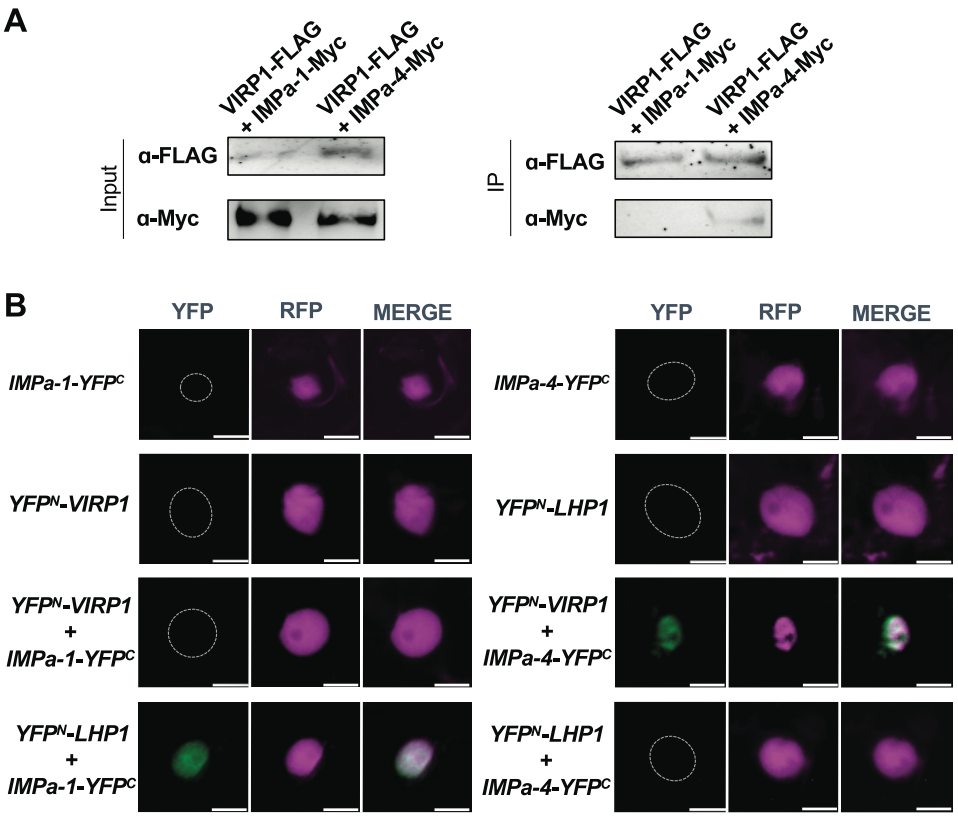

Figure 2 IMPa-4 and VIRP1 interaction in plants. A, Co-immunoprecipitation. Agroinfiltration-based transient expression of FLAG-tagged VIRP1 in *N. benthamiana* serves a bait to pull down co-expressed IMPa proteins with a TAP-tag. IP, immunoprecipitated fraction. B, BiFC. *Nicotiana benthamiana* seedlings were used for transient expression of various combinations of constructs via agroinfiltration. *35S:RFP-Histone2B* serves as a marker for the nucleus. Scale bar, 8 μm. White dashed lines outline the positions of nuclei.

plants infected with TRV^{vector} than those infected with TRV^{IMPa-4} (Figure 1E). We quantified fluorescence signals in more than 50 nuclei in 10 randomly picked areas from at least three plants of each treatment and found that the VIRP1-GFP signal reduction in TRV^{IMPa-4}-infected plants is statistically significant ($P < 0.0001$) based on two-tailed *t* test (Figure 1F).

To investigate the possible physical interactions between IMPa-4 and VIRP1, we employed the co-immunoprecipitation assay. Because VIRP1 expressed at a relatively low level in *N. benthamiana*, we used an estrogen-based inducible expression system (Zuo et al., 2000) to boost the expression of VIRP1. We transiently expressed a FLAG-tagged *VIRP1* construct together with TAP-tagged *IMPa-4* or *IMPa-1* via agroinfiltration. 17-b-estradiol was then supplied one day before sample collection. As shown in Figure 1C, VIRP1 interacted with IMPa-4 but not IMPa-1. We also performed bimolecular fluorescence complementation (BiFC) to further test the interaction between VIRP1 and IMPa-4. As shown in Figure 2B, agroinfiltration with a mixture of *35S:YFP^N-VIRP1* and *35S:IMPa-4-YFP^C* in *N. benthamiana* seedlings led to the detectable YFP fluorescence. In contrast, there was no YFP signal in cells co-expressing *35S:YFP^N-VIRP1* and *35S:IMPa-1-YFP^C* (Figure 2B). For BiFC assay, we also included LHP1 as an additional control. We observed YFP signals in *N. benthamiana* seedlings transiently co-expressing *35S:YFP^N-LHP1* and *35S:IMPa-1-YFP^C* but not cells co-expressing *35S:YFP^N-LHP1* and *35S:IMPa-4-YFP^C* (Figure 2B). These results support the idea that VIRP1 and IMPa-4 likely form a complex for nuclear import.

A 3D RNA motif mediates VIRP1 binding with PSTVd

Previous analysis suggested that VIRP1 binds to two possible RY motifs (R: A or G; Y: C or U) in PSTVd (Gozmanova et al., 2003), but the structural basis of the RY motif remains elusive. Furthermore, although a similar RY motif has been found in another nuclear-replicating viroid HSVd, the overall structures of the RY motif-containing regions between PSTVd and HSVd displayed significant differences (Gozmanova et al., 2003). A close look at the region containing RY motifs in PSTVd showed that there is a C-loop (loop 26) (Figure 3A). C-loop is an asymmetric internal loop, which has the following characteristic features: (1) the first base in the longer strand is often a C with some exceptions; (2) the longer strand has two bases forming non-WC–WC base pairings with bases in the other strand; (3) bases from two strands form two triads; and (4) this motif often resides in hairpin stem–loop structure (Lescoute et al., 2005; Drsata et al., 2017). Interestingly, our preliminary analysis showed that replacing the C-loop with WC–WC base pairs abolished

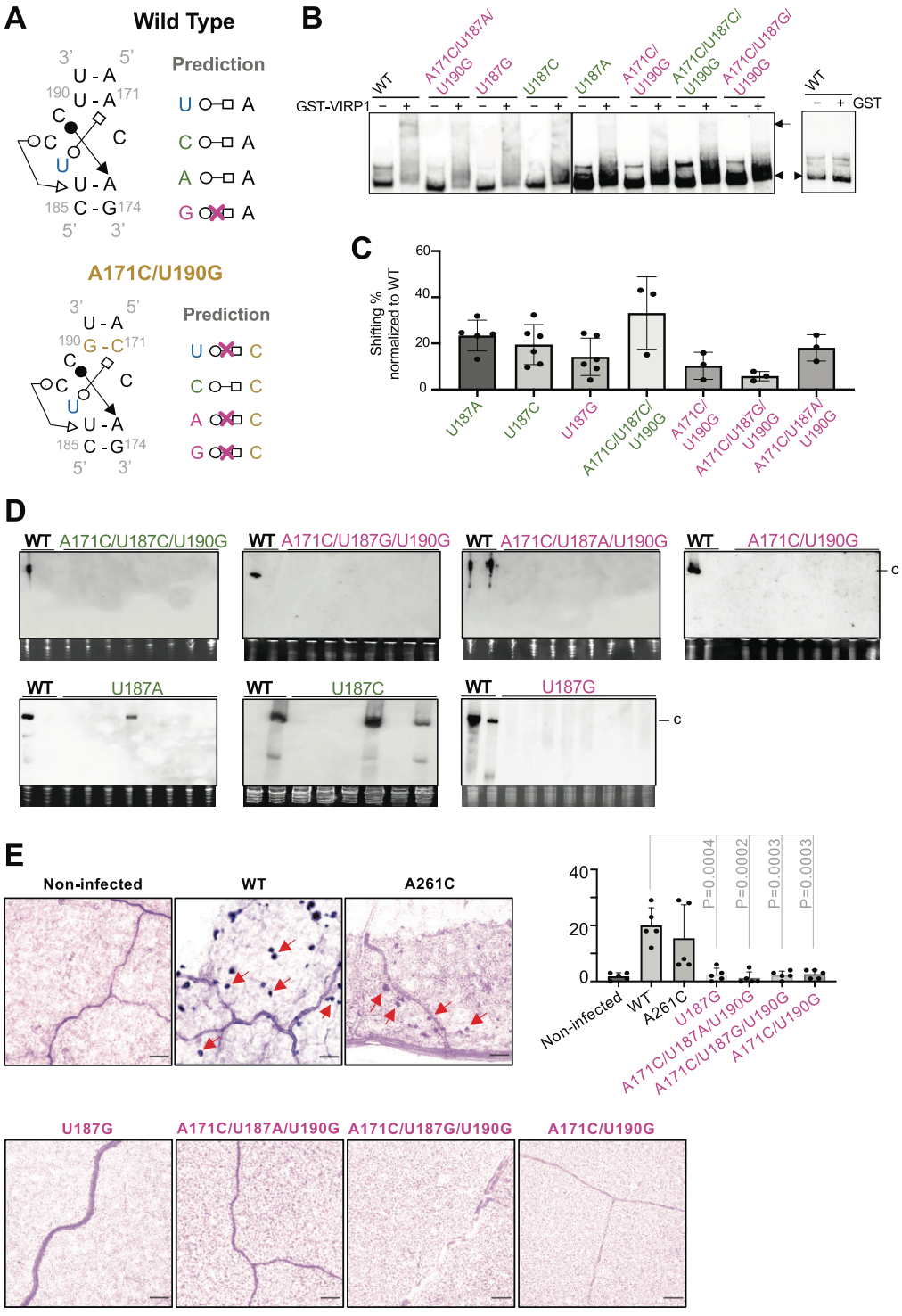

Figure 3 Characterizing PSTVd C-loop. A, Rationale for PSTVd C-loop mutagenesis. As explained in the Results, the critical trans-WC–Hoogsteen base pairing between A171 and U187 is subject to mutagenesis. Based on the RNA basepair catalog, structure-maintaining and structure-disruptive mutants were designed and highlighted in green and magenta, respectively. B, EMSA illustrating the interaction between C-loop mutants and VIRP1. Arrows and arrow heads indicate shifted RNA (in RNA–protein complex) and free RNA, respectively. C, Box plot showing quantification of EMSA results. The percent of RNA shifted in total RNA used for each reaction was calculated. The WT RNA shifted percentage was set as 100% in each replicate, and the mutant RNA shifted percentage was normalized to that of WT RNA. All C-loop mutants have a significant reduction in VIRP1 binding as compared with WT, based on two-tailed *t* test. D, RNA gel bots detecting PSTVd systemic infection in *N. benthamiana*. WT PSTVd serves as positive control. Ethidium bromide staining of rRNAs serves as loading control. c, circular PSTVd. E, Whole-mount in situ hybridization showing the presence of viroid RNAs in the nuclei (signal appears as purple dots). Scale bars, 72 μm. Arrows indicate examples of PSTVd-accumulated nuclei. Quantitative and statistical analyses of PSTVd-infected nuclei in similar visual areas from four plants of each treatment. There is no significant difference between noninfected and any of the C-loop mutant samples (*P*-value all >0.3).

PSTVd nuclear localization as observed by in situ hybridization analysis.

According to the C-loop model, PSTVd loop 26 is defined by two WC–WC base pairings (A171-U190 and A173-U186) on both ends. Within this potential C-loop, C189-A173 can form a cis-WC–Sugar base pair (cWS) and U187-A171 can form a trans-WC–Hoogsteen (tWH) base pair. The C189-A173 and U187-A171 base pairs, together with the WC–WC base pairs on both ends, form two triads (Supplemental Figure S1). C188 and U186 may form a trans-WC–Sugar base pair (tWS) as found in some but not all C-loop structures (Lescoute et al., 2005; Drsata et al., 2017). C172 is predicted as a free-standing base that is not involved in any base pairing. This PSTVd C-loop model is well supported by the chemical mapping data (Supplemental Figure S1; Xu et al., 2012; Lopez-Carrasco and Flores, 2017; Steger, 2017). Selective 2′-Hydroxyl Acylation analyzed by Primer Extension (SHAPE) assays from multiple studies using different chemicals collectively showed that C172 is highly reactive to modification in vitro and in vivo (Supplemental Figure S1), indicating that it is not involved in base pairing. In contrast, C189 consistently showed low reactivity in both in vitro and in vivo mapping assays (Supplemental Figure S1), demonstrating that it is involved in base-pairing. U187 showed medium reactivity in some of the mapping assays but low reactivity in others, which may be attributed to the loop "breathing" effect (Homan et al., 2014). This is further supported by the observation that the partner of U187, A171, also showed relatively high reactivity in some mapping experiments (Supplemental Figure S1). In summary, extensive chemical mapping experiments essentially support the idea that PSTVd loop 26 is a C-loop.

We employed mutational analyses as a genetic approach to further test whether loop 26 is a C-loop. Within the PSTVd C-loop (Figure 3A), the cWS base pairing between C189 and A173 as well as the tWS base-pairing between C188 and U186 are flexible for any nucleotide substitution in theory according to the RNA Basepair Catalog, so mutations in these two base pairings may not lead to any conclusive result. Instead, we designed substitutions to replace U187 that may or may not maintain similar tWH base pairing with A171. Alternatively, we replaced the U190-A171 cis-WC–WC base pair with G190-C171. Under this condition, U187 can only be substituted by C187 to maintain the tWH interaction with C171 according to the RNA Basepair Catalog. Using these mutational variants, we performed electrophoretic mobility shift assays (EMSAs) using recombinant VIRP1. Interestingly, VIRP1 only displayed a strong binding to wild-type (WT) PSTVd in EMSA (Figure 3, B and C), and structure-maintaining variants have relatively stronger binding to VIRP1 as compared with structure-disruptive variants (Figure 3C).

C-loop is critical for the infectivity and nuclear import of PSTVd

In attempt to determine the biological functions of C-loop in PSTVd, we analyzed the infectivity of C-loop mutants. As shown in Figure 3D, all PSTVd C-loop disruptive variants and one structure-maintaining mutant (A171C/U187C/U190G) failed to systemically infect *N. benthamiana*. All these infection-defective mutants have a weaker binding to VIRP1. Two structure-maintaining mutants, U187A and U187C, showed systemic infection. A careful analysis of the RNA progeny in the systemic leaves revealed that none of the progeny maintained the original sequences as inoculum (Supplemental Table S2). Nevertheless, nuclear localization is the prerequisite to initiating replication before mutations occur. Therefore, our data imply that the PSTVd structure-maintaining mutants U187A and U187C probably possess the ability to enter the nucleus. Importantly, the data further support that PSTVd loop 26 is a C-loop, because only the variants predicted to maintain the C-loop structure have relatively stronger binding to VIRP1 and retain the capacity to initiate replication.

We then analyzed the local leaves inoculated with C-loop variants via whole-mount in situ hybridization, which is a well-established approach for analyzing viroid-infected nuclei (Zhu et al., 2002; Qi et al., 2004; Zhong et al., 2007; Takeda et al., 2011). As shown in Figure 3E, no signal could be confidently detected in local leaves inoculated with C-loop disruptive mutants (i.e. U187G, A171C/U190G, A171C/U187A/U190G, and A171C/U187G/U190G). The very few signals in those samples are likely background false-positives akin to those in the noninoculated control leaves, because the signals in C-loop mutant-infected samples and in the negative control had no significant differences in *t* test (*P*-values all above 0.3) (Figure 3E). The structure-maintaining mutants (U187A and U187G) were not included in this assay because we cannot distinguish the original inoculum and replication products with mutations in whole-mount in situ hybridization assay. In contrast, WT PSTVd resulted in significantly more infected nuclei than any of the mutant-inoculated samples (*P*-values all <0.0005) (Figure 3E). The replication-deficient A261C mutant of PSTVd, which still has nuclear import ability (Zhong et al., 2006), showed detectable nuclear accumulation as well (Figure 3E). The nuclear accumulation signal of A261C in whole-mount in situ hybridization demonstrated that this assay is sensitive enough to capture imported inoculum without replication.

The lack of signal of C-loop disruptive mutants is unlikely caused by RNA stability, as we often observed C-loop variant inoculums in the local leaves 10-day postinfection. To further test RNA stability, we used agroinfiltration to deliver the cDNAs of C-loop variants into *N. benthamiana* plants and detected the accumulations of their transcripts about three-fold higher than the A261C transcripts as well as $>50\%$ as compared with the WT transcripts (Supplemental Figure S2). Altogether, the whole-mount in situ hybridization results support that the C-loop disruptive mutants lost their nuclear import ability. Therefore, C-loop likely plays an important role in nuclear import and full infectivity of PSTVd.

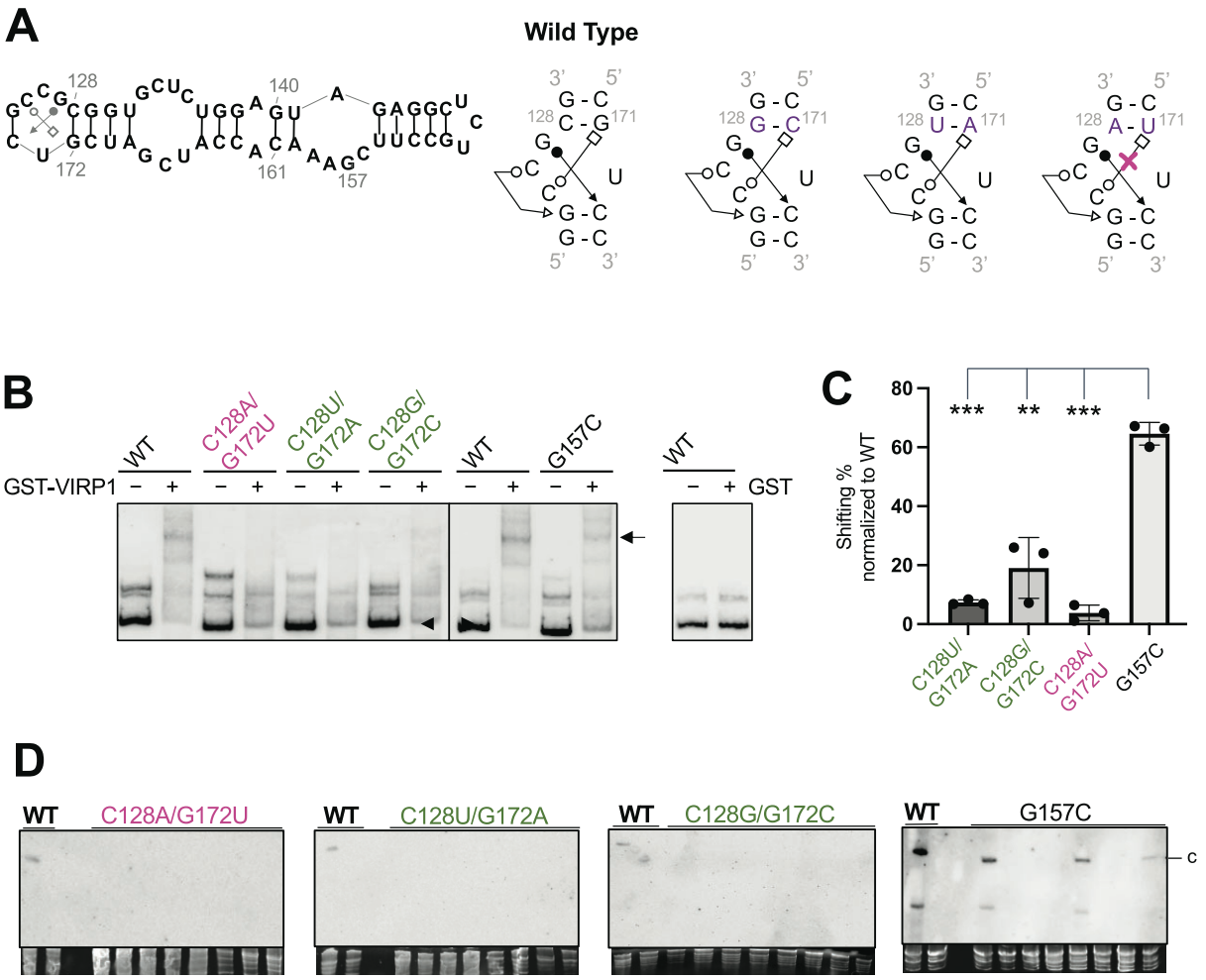

Figure 4 Characterizing a C-loop variant in HSVd. A, Rationale for HSVd C-loop mutagenesis. The critical trans-WC–Hoogsteen base pairing between C125 and G172 is subject to mutagenesis. Based on the RNA basepair catalog, C125–G172, C125–C172, C125–A172 but not C125–U172 can form the critical tWH pairing. The magenta cross depicts the structure-destructive design. B, EMSA illustrating the interaction between C-loop mutants and VIRP1. Arrowheads indicate the position of free probe, while the arrow indicates the position of RNA–protein complex. Multiple bands in "RNA only" lanes are likely caused by different confirmations of RNAs. C, Box plot showing quantification of EMSA results. Normalization method was the same as described in Figure 3. All C-loop mutants have a significant reduction in VIRP1 binding as compared with WT and G157C RNA, based on two-tailed *t* test. $^{**}P < 0.1$. $^{***}P < 0.001$. D, RNA gel bots detecting HSVd systemic infection in *N. benthamiana*. WT HSVd serves as positive controls. Ethidium bromide staining of rRNAs serves as loading control. c, circular genomic HSVd. Green and magenta colors depict structure-maintaining and structure-disruptive mutants, respectively.

C-loops occur widely in nuclear-replicating viroids

Notably, the C-loop can be found in 27 out of 28 formal members and three candidate members of the family *Pospiviroidae* (Supplemental Figure S3). Based on sequence variations and genomic coordination, we can categorize those viroids into two groups (Supplemental Figure S3). One group covers 11 viroids (including PSTVd), which all contain the same C-loop with identical genomic localization. The other group contains 19 viroids, which have C-loop structures with diverse sequence variations and genomic localization patterns (Supplemental Figure S3). This observation indicates that the C-loop is likely a common motif exploited by viroids for nuclear import.

Notably, we also found a variant version of C-loop in HSVd (Figure 4A), a PSTVd relative that has a slightly weaker binding to VIRP1 (Maniataki et al., 2003). To test this C-loop variant, we replaced the C128-G172 cis-WC–WC base pair with G–C, A–U, or U–A (Figure 4A). Only the A128-U172 substitution is predicted to disrupt the tWH base pair within the C-loop. Again, all HSVd C-loop mutants, including one structure-disruptive and two structure-maintaining mutants, exhibited much-reduced binding to VIRP1 (Figure 4, B and C). Both structure-maintaining mutants exhibited a slightly stronger binding to VIRP1 as compared with the structure-disruptive mutant. Since we observed reduced binding in all the mutational designs, one more mutant (G157C), which affects an adjacent loop to the C-loop in HSVd, was included as a control. This mutant now had significantly stronger binding to VIRP1 as compared with the binding between VIRP1 and HSVd C-loop mutants (Figure 4, B and C).

When we used HSVd C-loop mutants and the G157C mutant to infect *N. benthamiana* plants, only G157C accomplished successful infection (Figure 4D). Sequencing of the progeny confirmed that the G157C mutation was retained in the progeny in systemic leaves (Supplemental Table S2). Altogether, our observation supports that C-loop is critical for HSVd infectivity and VIRP1 specifically recognizes HSVd C-loop. Since structure-maintaining mutants also showed weak binding to VIRP1, it implies the existence of additional selection pressure that prefers certain nucleotides in composition of the C-loop.

Discussion

Proper subcellular localization dictates the function of biomolecules, including various cellular and infectious RNAs. While a majority of cellular RNAs are generated in the nucleus and then either stay in the nucleus or are transported to the cytoplasm for function, more and more RNAs were found to traffic in the reverse direction from the cytoplasm to the nucleus; these RNAs participate in diverse biological processes (Rudt and Pieler, 1996; Chou et al., 1998; Gao et al., 2012; Ye et al., 2012; Kramer and Hopper, 2013; Chaturvedi et al., 2014; Long et al., 2021). However, the mechanism underlying RNA nuclear import is poorly understood. Here, we present evidence supporting an IMPa-4-based cellular pathway, together with the cellular protein VIRP1, in transporting pathogenic noncoding RNAs (i.e. viroids) from the cytoplasm to the nucleus in plants (Figure 5). Based on the prediction using cNLS mapper (Kosugi et al., 2009a), *VIRP1* cloned from *A. thaliana* possesses two nuclear localization signals (NLSs), corresponding to amino acids (aa) 135–145 (LGPKKKKQKKN) and aa 397–427 (KDPNKRLMTMEEKSKLGMNLQDLPPEKLGOL). NLSs are normally recognized by importins (Conti et al., 1998; Harel and Forbes, 2004; Lange et al., 2007; Kosugi et al., 2009b). Considering that VIRP1 can directly bind viroid RNAs (Figures 3, B and 4, B) and is probably transported to the nucleus by IMPa-4-based cellular pathway, a reasonable model is that IMPa-4 recognizes the VIRP1–viroid complex for nuclear import (Figure 5).

We identified one genetic element, an RNA C-loop, as a critical signal for viroid nuclear import. PSTVd C-loop model is supported by chemical mapping data (Supplemental Figure S1) and functional mutagenesis-based genetic analyses. Disrupting C-loop impaired binding with VIRP1, inhibited nuclear accumulation of viroids in inoculated leaves, and compromised systemic infectivity. The absence of nuclear signal in whole-mount in situ hybridization using C-loop mutant-inoculated samples is unlikely caused by RNA instability. This is based on the observation that (1) C-loop mutants all had at least more than 50% accumulation levels as compared with WT RNA and (2) C-loop mutants all had significantly higher accumulation levels as compared with the replication-deficient A261C mutant that was detectable in whole-mount in situ hybridization (Supplemental Figure S2). Previous studies suggest that VIRP1 recognizes RY motifs in viroids (Gozmanova et al., 2003; Maniataki et al., 2003). The RY motif and C-loop partially overlap in some viroids, such as PSTVd. The drastic changes in binding and infectivity caused by point mutations in the PSTVd C-loop support the essential role of C-loop for VIRP1 recognition. More importantly, HSVd C-loop disruptive mutants that are not overlapping with RY motifs have a strong effect on infectivity and VIRP1 binding. In contrast, the G157C mutant that overlaps with the HSVd RY-motif retains infectivity and VIRP1-binding ability. Altogether, our data strongly support C-loop as a bona fide signal for selective nuclear import of RNA.

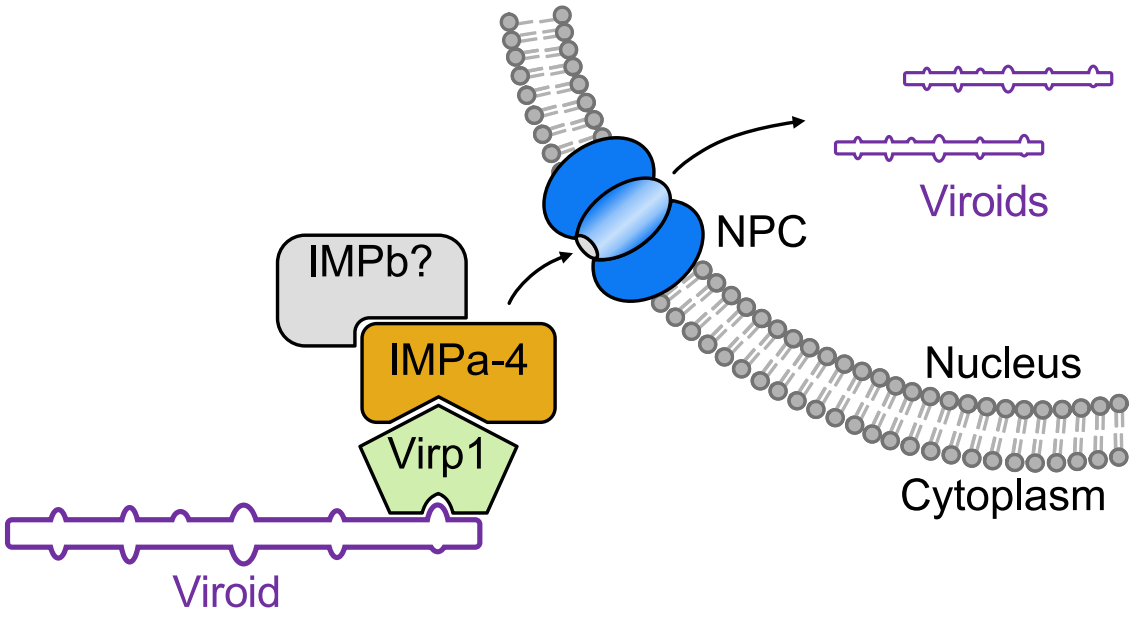

Figure 5 A working model illustrating the IMPa-4/VIRP1/C-loop-based RNA nuclear import. VIRP1 recognizes viroid C-loop to form an RNP complex, which is transported into the nucleus by IMPa-4. The IMPb responsible for viroid nuclear import remains to be identified.

C-loop has been found in many rRNAs (Lescoute et al., 2005; Drsata et al., 2017), a bacterial mRNA (Torres-Larios et al., 2002), and some conserved mammalian noncoding RNAs (Iacoangeli and Tiedge, 2013). In general, C-loop increases the local helical twist of RNA helices for protein binding (Afonin and Leontis, 2006). Studies showed that C-loop in the mRNA and those mammalian noncoding RNAs are involved in translational regulation (Torres-Larios et al., 2002; Iacoangeli and Tiedge, 2013). Our data not only expand the function of the C-loop but also uncover a new protein partner (i.e. VIRP1) for this RNA motif.

VIRP1 was first identified as a PSTVd-interacting protein by screening a cDNA library from PSTVd-infected tomato for RNA ligand binding (Martinez de Alba et al., 2003). Early work suggests that VIRP1 is important for PSTVd systemic trafficking because the binding-deficient PSTVd mutants failed to achieve systemic trafficking (Maniataki et al., 2003). Later on, protoplast assay using *VIRP1* downregulated cells suggested that *VIRP1* has a role in PSTVd replication (Kalantidis et al., 2007). Very recently, *VIRP1* has been implicated in regulating CEVd nuclear import in an in situ assay based on onion cells (Seo et al., 2021). Our results provide compelling evidence supporting a critical role of *VIRP1* in viroid nuclear import. Given that both *IMPa-4* and *VIRP1* have been implicated in *Agrobacterium tumefaciens* T-DNA nuclear import (Crane and Gelvin, 2007; Bhattacharjee et al., 2008), it will be interesting to further investigate whether *IMPa-4* and *VIRP1* also participate in the nuclear import of viral DNAs and/or cellular nucleic acids in the future.

There are 28 formal members of the family *Pospiviroidae* (Di Serio et al., 2021), and 27 of them (except citrus dwarfing viroid) possess a C-loop. Eleven viroids, including eight out of nine members in the genus *Pospiviroid*, which PSTVd belongs to, possess an identical C-loop in their genomes. Interestingly, the rest of the viroids in the *Pospiviroidae* family also carry a C-loop with some variations in sequences and genome localizations, except citrus dwarfing viroid (Supplemental Figure S3). Notably, these viroid genomic structures are supported by SHAPE analyses (Xu et al., 2012; Giguere et al., 2014; Giguere and Perreault, 2017), except for citrus bark cracking viroid and citrus viroid-VI whose structures were predicted using mFOLD (Zuker, 2003). Moreover, C-loop variants can also be found in Mexican papita viroid, citrus viroid-IV, and grapevine latent viroid, which are candidate members of *Pospiviroidae*. Therefore, a conserved nuclear import signal likely exists in nearly all nuclear-replicating viroids. Future functional investigation on those C-loop variants can provide insights into the precise structural basis and critical nucleotide preferences in mediating RNA nuclear import. It is also interesting to analyze citrus dwarfing viroid to test (1) whether it possesses an alternative binding site for VIRP1 and/or (2) whether there is an alternative nuclear import route.

Notably, Q-satRNA appears to have a C-loop in its RNA sequence as well. EMSA testing using a C-loop disruptive Q-satRNA showed significantly reduced binding to VIRP1 as compared with that of WT Q-satRNA ($P = 0.0012$), further supporting the critical role of C-loop in binding with VIRP1 (Supplemental Figure S4). Therefore, C-loop-based RNA nuclear import is possibly exploited by infectious RNAs in common. Whether any cellular RNA follows this pathway for nuclear import to exert functions in plants deserves future investigation. Our study paves the way to explore RNA nuclear import machinery and outlines a model for structural motif-based RNA subcellular localization. This line of research may lead to a comprehensive understanding of the accurate localization of RNAs in cells and future manipulation of subcellular localizations of various RNAs for functional studies and applications.

Materials and methods

Plant growth

Arabidopsis thaliana plants were grown in a growth chamber at 22°C with a 10-h/14-h light/dark cycle. *Nicotiana benthamiana* and tomato (*S. lycopersicum*) plants were grown in a growth chamber at 25°C with a 14-h/10-h light/dark cycle. Miracle-Gro all-purpose garden soil from a local Lowes store was used for plant growth. *N. benthamiana* and tomato seedlings at the four-leaf stage were inoculated with water or water containing 150 ng of in vitro-transcribed viroid RNAs. The viroid infection was analyzed by RNA gel blots using systemic leaves 3-week postinoculation. Agroinfiltration was performed following our established protocol (Wang et al., 2016).

DNA clones

cDNAs of some Arabidopsis IMPas in pC-TAPa or Lic6 vectors were purchased from ABRC (Ohio State University, Columbus, OH, USA): *IMPa-1* (DKLAT3G06720), *IMPa-2* (DKLAT4G16143), *IMPa-3* (DKLAT4G02150), *IMPa-4* (DKLAT1G09270), *IMPa-5* (DKLAT5G49310.1), and *IMPa-6* (DKLAT1G02690). *IMPa-7* cDNA in pDONR221 vector (DQ446636) was purchased from ABRC and recombined into pC-TAPa vector (ABRC) via LR clonase (Thermo Fisher Scientific, Waltham, MA, USA). *IMPa-8* and *IMPa-9* were cloned using gene-specific primers (Supplemental Table S3) via RT-PCR and inserted into pCR8 (Thermo Fisher Scientific), which were then recombined into pC-TAPa via LR clonase. It is noteworthy that the TAP tag in pC-TAPa contains 9X c-Myc tag, a His6 tag, and two IgG binding domains (Rubio et al., 2005). For BiFC, the *IMPa-1* and *IMPa-4* cDNAs in the entry vector were recombined into CD3-1651 (ABRC) using LR clonase.

To generate the pTRV2^{IMPa-4} clone, two specific primers (Supplemental Table S3) for *N. benthamiana IMPa-4* fragment were used for genomic PCR and followed by digestion with BamHI and XhoI (New England Biolabs, Ipswich, MA, USA). The pTRV2^{vector} (CD3-1040) was obtained from ABRC. After linearization by BamHI and XhoI, pTRV2^{vector} was used for ligation with the digested Nb *IMPa-4* fragments. Since we cannot reach 100% PSTVd infection in *N. benthamiana*, we then decided to use tomato for the

virus-induced gene silencing assay to assess the impact of *VIRP1* expression on PSTVd infectivity. Based on the high sequence similarity of *IMPa-4* in tomato and *N. benthamiana*, we used the same pTRV2^{IMPa-4} clone for infiltration of tomato. Based on the BLAST search using Sol genomics database (https://solgenomics.net), our cloned fragment specifically targets *IMPa-4* orthologs in tomato and *N. benthamiana*. pTRV2^{GFP} (CD3-1044) was obtained from ABRC. pTRV2 variants in agrobacterium GV3101 were mixed with agrobacterium harboring pTRV1 (ABRC) for infiltration into the first pair of true leaves of tomato seedlings, while cotyledons were used for inoculation with PSTVd RNA transcripts. Plants were subjected to RNA gel blots to analyze PSTVd and TRV titers, as well as RT-PCR for analyzing the expression levels of *IMPa-4* and *Histone H2A* (see Supplemental Table S3 for primer details). The TRV probe was described previously (Zheng et al., 2017b).

VIRP1 and *LHP1* from Arabidopsis were cloned via reverse transcription (RT)-PCR using gene-specific primers (Supplemental Table S3). The cloned cDNAs were inserted into pENTR-D-TOPO vector (Thermo Fisher Scientific) and then recombined into CD3-1637 (ABRC) or pMDC7 vector (modified to include a N-FLAG tag; inherited from Biao Ding at Ohio State University) for agroinfiltration, pDEST15 vector (Thermo Fisher Scientific) for bacterial expression or CD3-1648 (ABRC) for BiFC, via LR clonase. The construct for expressing free GST in bacteria was a gift from Svetlana Folimonova at University of Florida.

The cDNAs of WT and mutant Q-satRNAs were commercially synthesized (Genscript, Piscataway, NJ, USA). The cDNAs were amplified (see Supplemental Table S3 for primer sequences) and ligated into pGEM-T vector (Promega, Madison, WI, USA). To generate RNA substrates for EMSA, SpeI (New England Biolabs) linearized plasmids (pGEMT-Q-satRNA^{WT} and pGEMT-Q-satRNA^{mu}) were subject to in vitro transcription using T7 MEGAscript kit (Thermo Fisher Scientific).

To generate RNA inocula, pRZ:Int construct (Wang et al., 2007) was linearized by *Hin*dIII (New England Biolabs) followed by in vitro transcription using T7 MEGAscript kit. pT3:HSVd^{RZ} (Tu HSVd2-7 in the 83-82 orientation) used pGEM-T vector with the insertion cloned from HSVd-RZ (a gift from Robert Owens at USDA-ARS) via T3-HSVd-f and RZ-r primers (Supplemental Table S3). pT3:HSVd^{RZ} was linearized by *Hin*dIII followed by *in vitro* transcription using T3 MEGAscript kit (Thermo Fisher Scientific). All RNA in vitro transcripts were purified using the MEGAclear kit (Thermo Fisher Scientific).

To generate riboprobes, pInt(-) (Dissanayaka Mudiyanselage and Wang, 2020) was linearized by *Spe*I (New England Biolabs) as the template and T7 MAXIscript kit (Thermo Fisher Scientific) was used to generate probe. pHSVd-monomer was based on pGEM-T vector (Promega) via insertion of HSVd cDNA cloned from HSVd-RZ plasmid via HSVd-f and HSVd-r primers (Supplemental Table S3). The pHSVd-Monomer was linearized by NcoI (New England Biolabs) as the template and SP6 MAXIscript kit (Thermo Fisher Scientific) was used to generate probe. To generate Q-satRNA probe, pGEMT-Q-satRNA^{WT} was linearized by NcoI (New England Biolabs) and subject to in vitro transcription using SP6 MAXIscript kit.

To generate WT, A261C, and C-loop mutant constructs for agroinfiltration, the corresponding pRZ:Int plasmids harboring the corresponding PSTVd cDNAs served as templates for PCR (using RZ-f and RZ-r primers; see Supplemental Table S3 for primer sequences). The PCR products were inserted into pENTR-D-TOPO vector (Thermo Fisher Scientific). The series of pENTR-RZ:Int plasmids were recombined into CD3-1656 (ABRC) via LR clonase. The CD3-1656-RZ:Int plasmid series were transformed into Agrobacterium strain GV3101 for agroinfiltration.

All the constructs have been verified using Sanger sequencing.

RNA immunoprecipitation

RNA immunoprecipitation was performed according to a previously described protocol (Wang et al., 2016) with minor modifications. Briefly, PSTVd-infected *N. benthamiana* leaves were harvested 3-day postagroinfiltration of *IMPa* cDNAs. The cell lysates were incubated with magnetic mouse IgG beads (catalog #5873; Cell Signaling, Danvers, MA, USA) for 2 h at 4°C. The input lysate and purified fractions were subject to immunoblotting and RT-PCR (after Trizol-based RNA purification). The primers for detecting PSTVd and *Histone 2A* mRNA were listed in Supplemental Table S3. RNA immunoprecipitation experiments were repeated at least twice for each *IMPa* gene. For each biological replicate, mixed leaf tissues from three or more plants were used for each treatment.

Co-immunoprecipitation

Co-immunoprecipitation was following a recent report (Chen et al., 2020) with minor modifications. FLAG-tagged *VIRP1* with an estrogen-inducible promoter was co-expressed transiently with TAP-tagged *IMPa-1* or *IMPa-4* via agroinfiltration in *N. benthamiana*. Three days postinfiltration, 4-mM 17-b-estradiol was infiltrated into leaves 6 h before sampling. The cell lysates from leaf samples were incubated with anti-FLAG antibody (catalog #MA1-142; Thermo Fisher Scientific) for 1 h at 4°C. The magnetic protein A/G beads (catalog #88802; Thermo Fisher Scientific) were then added to the lysate for another 1-h incubation at 4°C with mild shaking. The beads were washed twice with 1 × PBST buffer (137-mM NaCl, 2.7-mM KCl, 10-mM Na_2HPO_4, 1.8-mM KH_2PO_4, 0.1% Triton X-100) and once with distilled water. The bound proteins were eluted using IgG elution buffer (Thermo Fisher Scientific) and then subject to immunoblots. Co-immunoprecipitation experiments were repeated twice. For each biological replicate, mixed leaf tissues from three or more plants were used for each treatment.

Protein purification

GST and Recombinant VIRP1-GST proteins were expressed in *Escherichia coli* Rosetta strain (EMD Millipore, Burlington, MA, USA). Cells were grown overnight at 37°C in LB media supplied with ampicillin (100 μg mL^{-1}) and chloramphenicol (34 μg mL^{-1}). An aliquot of cells with optical density at 600 nm (OD_{600}) = 0.1 was inoculated into fresh LB supplied with antibiotics the next day. Once the cell density (OD_{600}) reached 0.5–0.7, 0.4-mM IPTG (final concentration) was added to the culture to induce protein expression. After inducing at 20°C overnight, 100-mL culture was harvested by centrifugation at 8,000 *g* for 8 min. Pellets were re-suspended in 1 × PBS buffer (137-mM NaCl, 2.7-mM KCl, 10-mM Na_2HPO_4, and 1.8-mM KH_2PO_4) supplement with 20-mM PMSF and sonicated to lyse the cells. The cell lysate was then centrifuged at 10,800 *g* for 30 min at 4°C. The supernatant was collected and incubated for 1 h with 50% slurry of Glutathione Resin (Genscript) before loading onto an empty EconoPac gravity-flow column (Bio-Rad Laboratories, Hercules, CA, USA). The resin was then washed with 10 mL 1 × PBS followed by applying 10-mL elution buffer (50-mM Tris–HCl pH 8.0 and 10-mM reduced glutathione). The elutes were concentrated using an Amicon protein concentrator (MilliporeSigma, Burlington, MA, USA). Proteins were then separated by 8% sodium dodecyl-sulfate polyacrylamide gel electrophoresis (SDS–PAGE) electrophoresis followed by Coomassie blue staining and de-staining to estimate concentration using a BSA standard as reference.

EMSAs

EMSAs were conducted following a previously reported protocol (Gozmanova et al., 2003). Binding assays that contained RNA in the absence or presence of different amounts of GST or VIRP1-GST proteins were incubated at 28°C for 30 min. The binding buffer was composed of 10-mM HEPES-NaOH (pH 8.0), 50-mM KCl, 100-mM EDTA, and 5% glycerol. Electrophoresis for the binding assay was performed on ice in 6% polyacrylamide (29:1) gels at 140 V using 0.5 × TBE (50-mM Tris, 50-mM boric acid, 1-mM EDTA, and pH 8.3) for 1.6 h. The following steps are described below in the RNA gel blots section. The percentage of shifted variant RNAs was normalized to that of WT RNAs to infer a relative binding strength to VIRP1, based on at least three biological replicates.

Tissue processing and in situ hybridization

The tissue fixation and processing were largely described previously (Takeda et al., 2011) with minor modifications. Briefly, *N. benthamiana* leaf samples (8-day postinoculation) and tomato systemic leaves (3-week postinoculation) were collected and fixed in FAA solution (50% ethanol/5% formaldehyde/5% acetic acid) for 30 min and then dehydrated by a step-wise gradient of ethanol solutions (50%, 80%, 95%, and 100%). The samples were washed in 1 × PBS and treated with 10 mg mL^{-1} of proteinase K for 20 min at 37°C. Then, the samples were hybridized with digoxigenin (DIG)-labeled antisense riboprobes (generated as above-mentioned) at 50°C overnight. The samples were washed, incubated with anti-DIG monoclonal antibody (catalog #11333089001; MilliporeSigma) and NBT/BCIP substrate (MilliporeSigma) subsequentially, and mounted with Permount (Thermo Fisher Scientific) for visualization using an Olympus CX23 light microscope. The scale bars were calculated using ImageJ (https://imagej.nih.gov/ij/). Samples were collected from at least four plants for each treatment.

RNA gel blots and immunoblots

After electrophoresis, RNAs were then transferred to Hybond-XL nylon membranes (Amersham Biosciences, Little Chalfont, UK) via a semi-dry transfer cassette (Bio-Rad Laboratories) and were immobilized by a UV-crosslinker (UVP, Upland, CA, USA). RNAs were then detected by DIG-labeled UTP probes. AP-conjugated anti-DIG monoclonal antibody (catalog #11333089001; MilliporeSigma) was used in combination with Immun-Star substrates (Bio-Rad Laboratories). Signals were captured by ChemiDoc (Bio-Rad Laboratories).

After SDS–PAGE electrophoresis, we followed a previously described protocol for immunoblotting (Jiang et al., 2019). IMPas were detected by a monoclonal mouse anti-Myc antibody (catalog #M5546; MilliporeSigma; 1:3,000 dilution). VIRP1 was detected by a monoclonal mouse anti-FLAG antibody (catalog #F1804-200UG; MilliporeSigma; 1:1,000 dilution). HRP-conjugated anti-mouse serum (catalog #1706516; Bio-Rad Laboratories) was diluted at 1:2,000. SuperSignal West Dura (Thermo Fisher Scientific) was used as the substrate. Signals were captured by ChemiDoc (Bio-Rad Laboratories).

BiFC and microscopy

For BiFC, *N. benthamiana* seedlings were used for agroinfiltration of various combinations of constructs, all including *35S:RFP-Histone 2B* (Yang et al., 2011) as the nucleus marker. The N split (aa 1–174) *YFP* was fused in front of the N-terminus of *LHP1* or *VIRP1*. The C split *YFP* (aa 175-end) was fused after the C-terminus of *IMPa-1* or IMPa-4. For GFP-fusion proteins, we used agroinfiltration for transient expression in *N. benthamiana* seedlings and DAPI staining to indicate the nucleus following our established method (Wang et al., 2016). We analyzed 10 randomly chosen regions of infiltrated leaves from at least three plants for each treatment. EVOS FL imaging system (Thermo Fisher Scientific) was used for observing the fluorescence expressed in plants. GFP channel was used for analyzing YFP and GFP with a fixed setting of lower illumination (30%) and a shorter exposure time (250 ms). LHP1-GFP and VIRP1-GFP signals were quantified using ImageJ. The quantification data were analyzed by the unpaired *t* test (two-tailed), using the built-in function in Prism (GraphPad Software, LLC).

Accession numbers

The published RNA-Seq dataset has been deposited in the NCBI SRA with accession number SRP093503. The accession numbers of *A. thaliana IMPa* genes are: At *IMPa-1*

(AT3G06720), At *IMPa-2* (AT4G16143), At *IMPa-3* (AT4G02150), At *IMPa-4* (AT1G09270), At *IMPa-5* (AT5G49310), At *IMPa-6* (AT1G02690), At *IMPa-7* (AT3G05720), At *IMPa-8* (AT5G52000), and At *IMPa-9* (AT5G03070). The accession numbers of tomato (*S. lycopersicum*) *IMPa* genes are Sl *IMPa-1* (Solyc08g041890), Sl *IMPa-2* (Solyc01g060470), Sl *IMPa-3* (Solyc06g009750), Sl *IMPa-4* (Solyc01g100720), and Sl *IMPa-9* (Solyc10g084270), The accession numbers of *N. benthamiana IMPa-4* homologs are Niben101Scf01964g10002.1 and Niben101Scf04827g03005.1. The At *VIRP1* gene accession is AT5G65630. The accession numbers of PSTVd, HSVd, and Q-satRNA used in this study are AY937179, DQ371459, and J02060, correspondingly.

Supplemental data

The following materials are available in the online version of this article.

Supplemental Figure S1. SHAPE analyses supporting PSTVd C-loop model.

Supplemental Figure S2. The RNA stability of PSTVd C-loop variants.

Supplemental Figure S3. C-loop in nuclear-replicating viroids.

Supplemental Figure S4. VIRP1 interaction with Q-satRNA.

Supplemental Table S1. IMPa homologs in tomato.

Supplemental Table S2. PSTVd and HSVd progeny in systemic leaves.

Supplemental Table S3. Primer sequences.

Acknowledgments

We are grateful for the constructive comments from Donna Gordon (Mississippi State University). We thank Laxmi Kharel (Mississippi State University) for technical support. This work is dedicated to the late Professors Biao Ding (Ohio State University) and Neocles B. Leontis (Bowling Green State University), who participated at the inception stage. We are indebted to Robert Owens (USDA-ARS), David Bisaro (Ohio State University) and Svetlana Folimonova (University of Florida) for their gifts of DNA constructs.

Funding

This work was supported by grants from the US National Science Foundation (MCB-1906060 and MCB-2145967 to YW) and the US National Institute of General Medical Sciences (1R15GM135893 to YW).

Conflict of interest statement. None declared.

References

Afonin KA, Leontis NB (2006) Generating new specific RNA interaction interfaces using C-loops. J Am Chem Soc **128**: 16131–16137

Bhattacharjee S, Lee LY, Oltmanns H, Cao H, Veena, Cuperus J, Gelvin SB (2008) IMPa-4, an Arabidopsis importin alpha isoform, is preferentially involved in agrobacterium-mediated plant transformation. Plant Cell **20**: 2661–2680

Chaturvedi S, Kalantidis K, Rao AL (2014) A bromodomain-containing host protein mediates the nuclear importation of a satellite RNA of Cucumber mosaic virus. J Virol **88**: 1890–1896

Chen C, Kim D, Yun HR, Lee YM, Yogendra B, Bo Z, Kim HE, Min JH, Lee YS, Rim YG, et al. (2020) Nuclear import of LIKE HETEROCHROMATIN PROTEIN1 is redundantly mediated by importins alpha-1, alpha-2 and alpha-3. Plant J **103**: 1205–1214

Chou HC, Hsieh TY, Sheu GT, Lai MM (1998) Hepatitis delta antigen mediates the nuclear import of hepatitis delta virus RNA. J Virol **72**: 3684–3690

Conti E, Uy M, Leighton L, Blobel G, Kuriyan J (1998) Crystallographic analysis of the recognition of a nuclear localization signal by the nuclear import factor karyopherin alpha. Cell **94**: 193–204

Crane YM, Gelvin SB (2007) RNAi-mediated gene silencing reveals involvement of Arabidopsis chromatin-related genes in Agrobacterium-mediated root transformation. Proc Natl Acad Sci USA **104**: 15156–15161

Daros JA, Flores R (2004) *Arabidopsis thaliana* has the enzymatic machinery for replicating representative viroid species of the family Pospiviroidae. Proc Natl Acad Sci USA **101**: 6792–6797

Di Serio F, Owens RA, Li SF, Matousek J, Pallas V, Randles JW, Sano T, Verhoeven JTJ, Vidalakis G, Flores R, et al. (2021) ICTV virus taxonomy profile: pospiviroidae. J Gen Virol **102**: 001543

Dissanayaka Mudiyanselage SD, Wang Y (2020) Evidence supporting that RNA polymerase II catalyzes de novo transcription using potato spindle tuber viroid circular RNA templates. Viruses **12**: 371

Drsata T, Reblova K, Besseova I, Sponer J, Lankas F (2017) rRNA C-loops: mechanical properties of a recurrent structural motif. J Chem Theory Comput **13**: 3359–3371

Frey S, Gorlich D (2009) FG/FxFG as well as GLFG repeats form a selective permeability barrier with self-healing properties. EMBO J **28**: 2554–2567

Frey S, Richter RP, Gorlich D (2006) FG-rich repeats of nuclear pore proteins form a three-dimensional meshwork with hydrogel-like properties. Science **314**: 815–817

Gao R, Liu P, Wong SM (2012) Identification of a plant viral RNA genome in the nucleus. PLoS One **7**: e48736

Gast FU, Kempe D, Spieker RL, Sanger HL (1996) Secondary structure probing of potato spindle tuber viroid (PSTVd) and sequence comparison with other small pathogenic RNA replicons provides evidence for central non-canonical base-pairs, large A-rich loops, and a terminal branch. J Mol Biol **262**: 652–670

Giguere T, Perreault JP (2017) Classification of the Pospiviroidae based on their structural hallmarks. PLoS One **12**: e0182536

Giguere T, Adkar-Purushothama CR, Perreault JP (2014) Comprehensive secondary structure elucidation of four genera of the family Pospiviroidae. PLoS One **9**: e98655

Gozmanova M, Denti MA, Minkov IN, Tsagris M, Tabler M (2003) Characterization of the RNA motif responsible for the specific interaction of potato spindle tuber viroid RNA (PSTVd) and the tomato protein VIRP1. Nucleic Acids Res **31**: 5534–5543

Harel A, Forbes DJ (2004) Importin beta: conducting a much larger cellular symphony. Mol Cell **16**: 319–330

Homan PJ, Favorov OV, Lavender CA, Kursun O, Ge X, Busan S, Dokholyan NV, Weeks KM (2014) Single-molecule correlated chemical probing of RNA. Proc Natl Acad Sci USA **111**: 13858–13863

Iacoangeli A, Tiedge H (2013) Translational control at the synapse: role of RNA regulators. Trends Biochem Sci **38**: 47–55

Jiang J, Ma J, Liu B, Wang Y (2019) Combining a simple method for DNA/RNA/protein co-purification and Arabidopsis protoplast assay to facilitate viroid research. Viruses **11**: 324

Kalantidis K, Denti MA, Tzortzakaki S, Marinou E, Tabler M, Tsagris M (2007) VIRP1 is a host protein with a major role in Potato spindle tuber viroid infection in Nicotiana plants. J Virol **81**: 12872–12880

Kosugi S, Hasebe M, Tomita M, Yanagawa H (2009a) Systematic identification of cell cycle-dependent yeast nucleocytoplasmic shuttling proteins by prediction of composite motifs. Proc Natl Acad Sci USA **106**: 10171–10176

Kosugi S, Hasebe M, Matsumura N, Takashima H, Miyamoto-Sato E, Tomita M, Yanagawa H (2009b) Six classes of nuclear localization signals specific to different binding grooves of importin alpha. J Biol Chem **284**: 478–485

Kramer EB, Hopper AK (2013) Retrograde transfer RNA nuclear import provides a new level of tRNA quality control in Saccharomyces cerevisiae. Proc Natl Acad Sci USA **110**: 21042–21047

Lange A, Mills RE, Lange CJ, Stewart M, Devine SE, Corbett AH (2007) Classical nuclear localization signals: definition, function, and interaction with importin alpha. J Biol Chem **282**: 5101–5105

Lescoute A, Leontis NB, Massire C, Westhof E (2005) Recurrent structural RNA motifs, Isostericity Matrices and sequence alignments. Nucleic Acids Res **33**: 2395–2409

Long J, Walker J, She W, Aldridge B, Gao H, Deans S, Vickers M, Feng X (2021) Nurse cell–derived small RNAs define paternal epigenetic inheritance in Arabidopsis. Science **373**: eabh0556

Lopez-Carrasco A, Flores R (2017) Dissecting the secondary structure of the circular RNA of a nuclear viroid in vivo: a "naked" rod-like conformation similar but not identical to that observed in vitro. RNA Biol **14**: 1046–1054

Ma J, Wang Y (2022) Studies on viroid shed light on the role of RNA three-dimensional structural motifs in RNA trafficking in plants. Front Plant Sci **13**: 836267

Maniataki E, Martinez de Alba AE, Sagesser R, Tabler M, Tsagris M (2003) Viroid RNA systemic spread may depend on the interaction of a 71-nucleotide bulged hairpin with the host protein VIRP1. RNA **9**: 346–354

Martinez de Alba AE, Sagesser R, Tabler M, Tsagris M (2003) A bromodomain-containing protein from tomato specifically binds potato spindle tuber viroid RNA in vitro and in vivo. J Virol **77**: 9685–9694

Meier I, Brkljacic J (2009) Adding pieces to the puzzling plant nuclear envelope. Curr Opin Plant Biol **12**: 752–759

Merkle T (2011) Nucleo-cytoplasmic transport of proteins and RNA in plants. Plant Cell Rep **30**: 153–176

Qi Y, Pélissier T, Itaya A, Hunt E, Wassenegger M, Ding B (2004) Direct role of a viroid RNA motif in mediating directional RNA trafficking across a specific cellular boundary. Plant Cell **16**: 1741–1752

Rubio V, Shen Y, Saijo Y, Liu Y, Gusmaroli G, Dinesh-Kumar SP, Deng XW (2005) An alternative tandem affinity purification strategy applied to Arabidopsis protein complex isolation. Plant J **41**: 767–778

Rudt F, Pieler T (1996) Cytoplasmic retention and nuclear import of 5S ribosomal RNA containing RNPs. EMBO J **15**: 1383–1391

Sarver M, Zirbel CL, Stombaugh J, Mokdad A, Leontis NB (2008) FR3D: finding local and composite recurrent structural motifs in RNA 3D structures. J Math Biol **56**: 215–252

Seo H, Wang Y, Park WJ (2020) Time-resolved observation of the destination of microinjected potato spindle tuber viroid (PSTVd) in the abaxial leaf epidermal cells of *Nicotiana benthamiana*. Microorganisms **8**: 2044

Seo H, Kim K, Park WJ (2021) Effect of VIRP1 protein on nuclear import of citrus exocortis viroid (CEVd). Biomolecules **11**: 95

Steger G (2017) Modelling the three-dimensional structure of the right-terminal domain of pospiviroids. Sci Rep **7**: 711

Stewart CL, Roux KJ, Burke B (2007) Blurring the boundary: the nuclear envelope extends its reach. Science **318**: 1408–1412

Stombaugh J, Zirbel CL, Westhof E, Leontis NB (2009) Frequency and isostericity of RNA base pairs. Nucleic Acids Res **37**: 2294–2312

Takeda R, Petrov AI, Leontis NB, Ding B (2011) A three-dimensional RNA motif in Potato spindle tuber viroid mediates trafficking from palisade mesophyll to spongy mesophyll in *Nicotiana benthamiana*. Plant Cell **23**: 258–272

Takeda R, Zirbel CL, Leontis NB, Wang Y, Ding B (2018) Allelic RNA motifs in regulating systemic trafficking of potato spindle tuber viroid. Viruses **10**: 160

Torres-Larios A, Dock-Bregeon AC, Romby P, Rees B, Sankaranarayanan R, Caillet J, Springer M, Ehresmann C, Ehresmann B, Moras D (2002) Structural basis of translational control by Escherichia coli threonyl tRNA synthetase. Nat Struct Biol **9**: 343–347

Wang Y (2021) Current view and perspectives in viroid replication. Curr Opin Virol **47**: 32–37

Wang Y, Qu J, Ji S, Wallace AJ, Wu J, Li Y, Gopalan V, Ding B (2016) A land plant-specific transcription factor directly enhances transcription of a pathogenic noncoding RNA template by DNA-dependent RNA polymerase II. Plant Cell **28**: 1094–1107

Wang Y, Zhong X, Itaya A, Ding B (2007) Evidence for the existence of the loop E motif of potato spindle tuber viroid in vivo. J Virol **81**: 2074–2077

Wang Y, Zirbel CL, Leontis NB, Ding B (2018) RNA 3-dimensional structural motifs as a critical constraint of viroid RNA evolution. PLoS Pathog **14**: e1006801

Woo YM, Itaya A, Owens RA, Tang L, Hammond RW, Chou HC, Lai MMC, Ding B (1999) Characterization of nuclear import of potato spindle tuber viroid RNA in permeabilized protoplasts. Plant J **17**: 627–635

Wu J, Leontis NB, Zirbel CL, Bisaro DM, Ding B (2019) A three-dimensional RNA motif mediates directional trafficking of Potato spindle tuber viroid from epidermal to palisade mesophyll cells in *Nicotiana benthamiana*. PLoS Pathog **15**: e1008147

Xu W, Bolduc F, Hong N, Perreault JP (2012) The use of a combination of computer-assisted structure prediction and SHAPE probing to elucidate the secondary structures of five viroids. Mol Plant Pathol **13**: 666–676

Xu XM, Meier I (2008) The nuclear pore comes to the fore. Trends Plant Sci **13**: 20–27

Yang X, Xie Y, Raja P, Li S, Wolf JN, Shen Q, Bisaro DM, Zhou X (2011) Suppression of methylation-mediated transcriptional gene silencing by betaC1-SAHH protein interaction during geminivirus-betasatellite infection. PLoS Pathog **7**: e1002329

Ye R, Wang W, Iki T, Liu C, Wu Y, Ishikawa M, Zhou X, Qi Y (2012) Cytoplasmic assembly and selective nuclear import of Arabidopsis Argonaute4/siRNA complexes. Mol Cell **46**: 859–870

Zheng Y, Ding B, Fei Z, Wang Y (2017b) Comprehensive transcriptome analyses reveal tomato plant responses to tobacco rattle virus-based gene silencing vectors. Sci Rep **7**: 9771

Zheng Y, Wang Y, Ding B, Fei Z (2017a) Comprehensive transcriptome analyses reveal that potato spindle tuber viroid triggers genome-wide changes in alternative splicing, inducible trans-acting activity of phasiRNAs and immune responses. J Virol **91**: e00247-17

Zhong X, Archual AJ, Amin AA, Ding B (2008) A genomic map of viroid RNA motifs critical for replication and systemic trafficking. Plant Cell **20**: 35–47

Zhong X, Leontis N, Qian S, Itaya A, Qi Y, Boris-Lawrie K, Ding B (2006) Tertiary structural and functional analyses of a viroid RNA motif by isostericity matrix and mutagenesis reveal its essential role in replication. J Virol **80**: 8566–8581

Zhong X, Tao X, Stombaugh J, Leontis N, Ding B (2007) Tertiary structure and function of an RNA motif required for plant vascular entry to initiate systemic trafficking. EMBO J **26**: 3836–3846

Zhu Y, Qi Y, Xun Y, Owens R, Ding B (2002) Movement of potato spindle tuber viroid reveals regulatory points of phloem-mediated RNA traffic. Plant Physiol **130**: 138–146

Zirbel CL, Roll J, Sweeney BA, Petrov AI, Pirrung M, Leontis NB (2015) Identifying novel sequence variants of RNA 3D motifs. Nucleic Acids Res **43**: 7504–7520

Zuker M (2003) Mfold web server for nucleic acid folding and hybridization prediction. Nucleic Acids Res **31**: 3406–3415

Zuo J, Niu QW, Chua NH (2000) Technical advance: an estrogen receptor-based transactivator XVE mediates highly inducible gene expression in transgenic plants. Plant J **24**: 265–273